Ko-Fan ; **Ölualeg**; TaGküalsahnii gT;uK cehnijait a Wn;aPhonèli p Ki m



LowemTp. P49s.662-669 (2023)

https://doi.org/10.1063/10.0019423

Vi e w E x p o r t O n l i nCei t a t i o n

15 April 2024 02:17:03



The Beginner's Guide to Cryostats and Cryocoolers

A detailed analysis of cryogenic systems

Download guide ✓





Andreev reflection between aluminum and graphene across van der Waals barriers

Cite as: Fiz. Nizk. Temp. 49, 728-736 (June 2023); doi: 10.1063/10.0019423 Submitted: 27 April 2023







Ko-Fan Huang,¹ Önder Gül,¹ Takashi Taniguchi,² Kenji Watanabe,³ and Philip Kim^{1,a)}

AFFILIATIONS

- ¹Department of Physics, Harvard University, Cambridge, Massachusetts 02138, USA
- ²Research Center for Functional Materials, National Institute for Materials Science, Tsukuba, Japan
- ³International Center for Materials Nanoarchitectonics National Institute for Materials Science, Tsukuba, Japan
- ^{a)}Author to whom correspondence should be addressed: philipkim@g.harvard.edu

ABSTRACT

We present planar aluminum superconductor-graphene junctions whose hybrid interface is engineered for couplings ranging from tunneling to the strongly coupled regime by employing an atomically thin van der Waals tunneling barrier. Without the vdW barrier, we find Al makes strongly coupled contacts with the fully proximities graphene channel underneath. Using a large band gap hexagonal boron nitride (hBN) barrier, we find the junctions always remain in the weak coupling regime, exhibiting tunneling characteristics. Using monolayer semi-conducting transition metal dichalcogenides (TMDs) such as MoS2, we realize intermediate coupling with enhanced junction conductance due to the Andreev process. In this intermediate regime, we find that junction resistance changes in discrete steps when sweeping a perpendicular magnetic field. The period of the resistance steps in the magnetic field is inversely proportional to the junction area, suggesting the physical origin of our observations is due to magnetic-field-induced vortex formation in the planar junction. 02:17:03

Published under an exclusive license by AIP Publishing. https://doi.org/10.1063/10.0019423

1. INTRODUCTION

When a normal conductor is brought in close proximity to a superconductor, its properties can be dramatically changed. The early knowledge about this proximity effect was understood as the leakage of the superconducting order parameter from the superconductor into the normal region. A microscopic understanding of this physical mechanism can be described by the Andreev reflection¹ at the interface of a normal metal (N) and a superconductor (S). In this interfacial process, an electron in N is retro-reflected by a hole in N at the interface, creating a Cooper pair in S. The Andreev reflection describes how the electron is coherently reflected as a hole from the NS interface while a charge of -2e is transferred into the superconductor.

In a planar NS junction with arbitrary transparency of the NS interface, the Andreev process can be more quantitatively described by G. E. Blonder, M. Tinkham, and T. M. Klapwijk (BTK).² From the BTK model, we can show that the Andreev reflection probability is 100% for an ideal interface. Furthermore, this model includes the contribution of subgap conductance from Andreev reflection and is extremely useful for experimentalists studying transport through NS junctions.

Two-dimensional (2D) materials have been a uniquely versatile platform for induced superconductivity due to their electrostatic tunability, transparent interface, and atomically thin geometry allowing for a combination of metallic, semiconducting, and insulating planes while maintaining high mobility. Notable demonstrations include ballistic Josephson junctions,³ twist-interface-enabled superconductivity, and quantum Hall-superconductor hybrids.

To better understand the induced superconducting behaviors stemming from the superconducting contacts, one can rely on van der Waals (vdW) heterostructures in conjunction with 2D graphene channel. Depending on the vdW materials used as a barrier, one can explore different coupling regimes that the superconductivity proximity effect falls into, which are determined by the Andreev process probability.

In this work, we present planar aluminum superconductorgraphene junctions whose hybrid interface is engineered for couplings ranging from tunneling to the completely proximitized regime. For the junctions with weak coupling, we observe that the quasi-particle transport between Al and graphene is in the tunneling regime exhibiting conductance suppression. Without vdW barriers, Al superconducting electrode couples strongly with the

underlying graphene channel. We observe that no junction voltage is developed when Al remains superconducting. In the intermediate regime realized by the introduction of mono-layer TMDs between Al and graphene, we find that the junction shows staircase-like discrete changes in resistance when sweeping a perpendicular magnetic field, a behavior absent in the tunneling and strongly coupled junctions. We find that the period of the resistance steps is inversely proportional to the junction area.

2. EXPERIMENT

The van der Waals vertical structure is built by the inverted dry transfer technique.^{6,7} The bottom layer is a thick, clean flake of hBN (20-40 nm), creating a uniform substrate for graphene to minimize the disorder. On top of the graphene is the barrier layer that separates the evaporated Al superconducting electrode from the graphene channel layer. For this barrier, we chose atomically thin vdW materials so that the barrier thickness can be fine tuned on an atomic length scale. Within the van der Waals family, there exist many materials that range from insulating to semiconducting and then to completely conducting. Among them, we chose to use two as the interfacial layer: hBN and molybdenum disulfide (MoS_2) . These two mate-rials offer bandgaps of different sizes $(1.8\,eV$ for MoS_2 , 8 $6.1\,eV$ for $hBN^{9,10}$ which can help tune the contact transparency. Moreover, these materials frequently appear in large sizes after mechanical exfoliation. They also come in different thicknesses and can be in the thin limit with just a few atomic layers. These are important traits that allow us to fast-track the fabrication process.

For assembling vdW layers into the device structure shown in Fig. 1(a), we employ an inverted vdW stacking technique, 11 where the top surface of the stack is never in contact with any polymer

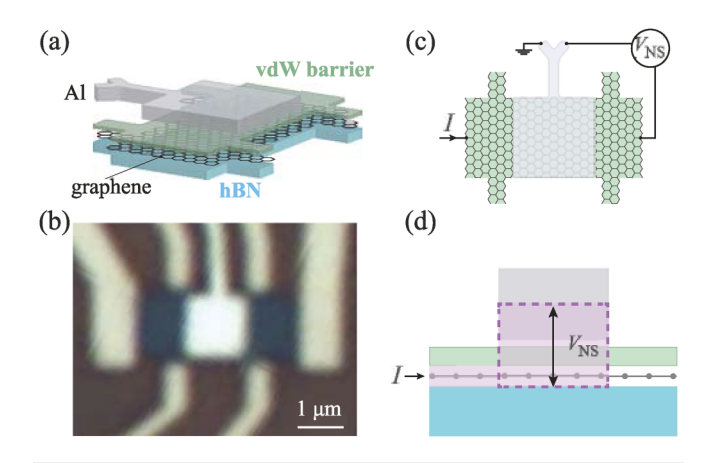


FIG. 1. (a) Illustration of the device structure, top and side view. The vdW barrier layer can be atomically thin hBN or TMDs. (b) Optical image of a typical device. (c) Measurement configuration of the vertical superconductor/barrier/graphene device structure. (d) Cross-sectional view of measurement configuration. The pink region denotes the current path (l) from a normal contact to graphene at one end to the Al contact. The voltage drop across the vertical junction V_{NS} the other end of the graphene to the Al lead.

layers for transferring. After the stack is assembled, the Hall-bar shaped geometry is defined followed by deposition of normal leads (5/50 nm of Cr/Au) [see Fig. 1(b)]. The device then undergoes the process of vacuum annealing at 350 °C for 15–20 minutes to remove any polymer residue from *e*-beam lithography, so that the tunnel path from graphene through the barrier layer to the superconductor is guaranteed to be clean. The final step is deposition of the superconducting contacts (5/80 nm of Ti/Al) on top of the area of interest.

The critical temperature of Al in the devices is typically around 1 K. All the measurements were performed in He3- fridge with a base temperature of 300 mK. The main focus is the graphene region underneath Al, where the superconducting proximity correlation is the strongest. As shown in Fig. 1(c), the Al contact branches out to two leads. The current (a small AC excitation dI on top of a DC bias current I_{bias}) is sent from a normal contact at the left end of graphene to the first Al lead, which is grounded. Then we measure the voltage $V_{\rm NS}$ between the other end of the graphene and the second Al lead. This is effectively the voltage drop across the vertical graphene-barrier-Al structure, as marked by the dotted square in Fig. 1(d). As a result, we obtain the tunneling conductance (or resistance) across the vertical NS junction, which characterizes the Andreev process in the system via the BTK model. With this measurement scheme, we categorize our devices into three regimes depending on the differential conductance profile as we discuss in the following sections.

3. STRONG COUPLING REGIME: AI/GRAPHENE

As a reference point in this study, we start with a device without any barrier layer–Al is deposited directly on top of graphene. The graphene in this type of device becomes fully proximized due to the highly strongly coupled su perconducting contact.

Figure 2(a) shows the differential resistance $dV/dI = dV_{\rm NS}/dE$ as a function of current bias ($I_{\rm bias}$) and back gate voltage V_{bg} . In the color plot, it is clear that there is a gap feature, in which the resistance drops to near zero (deep blue region), signifying the presence of superconductivity. At the Dirac peak of graphene, where $V_{bg} = 3$ V across 300 nm SiO₂ dielectric, the superconducting gap reaches a minimum. As the carrier density in graphene is increased, the gap becomes larger. This back-gate dependence suggests that dV/dI presented in this figure is related to the properties of graphene.

In Fig. 2(c), we plot the differential resistance as a function of current bias and applied magnetic field. In this figure, one can see how the induced gap (deep blue region)is measured from closes as the magnetic field approaches a critical field H_c . In addition, there are oscillations formed outside of the gap. These oscillations fan out from the superconducting gap and only exist in the superconducting regime (i.e., they also get quenched when the applied magnetic field rises above the critical field). We attribute these high bias conductance oscillations to the resonance of Andreev-process induced coherent mesoscopic states in either confined superconductor (Al islands) or normal metal (graphene channel). The Andreev process across the NS interface can lead to a periodic conductance modulation at finite bias voltage across the junction (i.e., outside of the superconducting gap) if the mesoscopic confinement induces quasi-particle interference within the superconducting region (Tomasch oscillations). 12-14 Similar periodic conductance

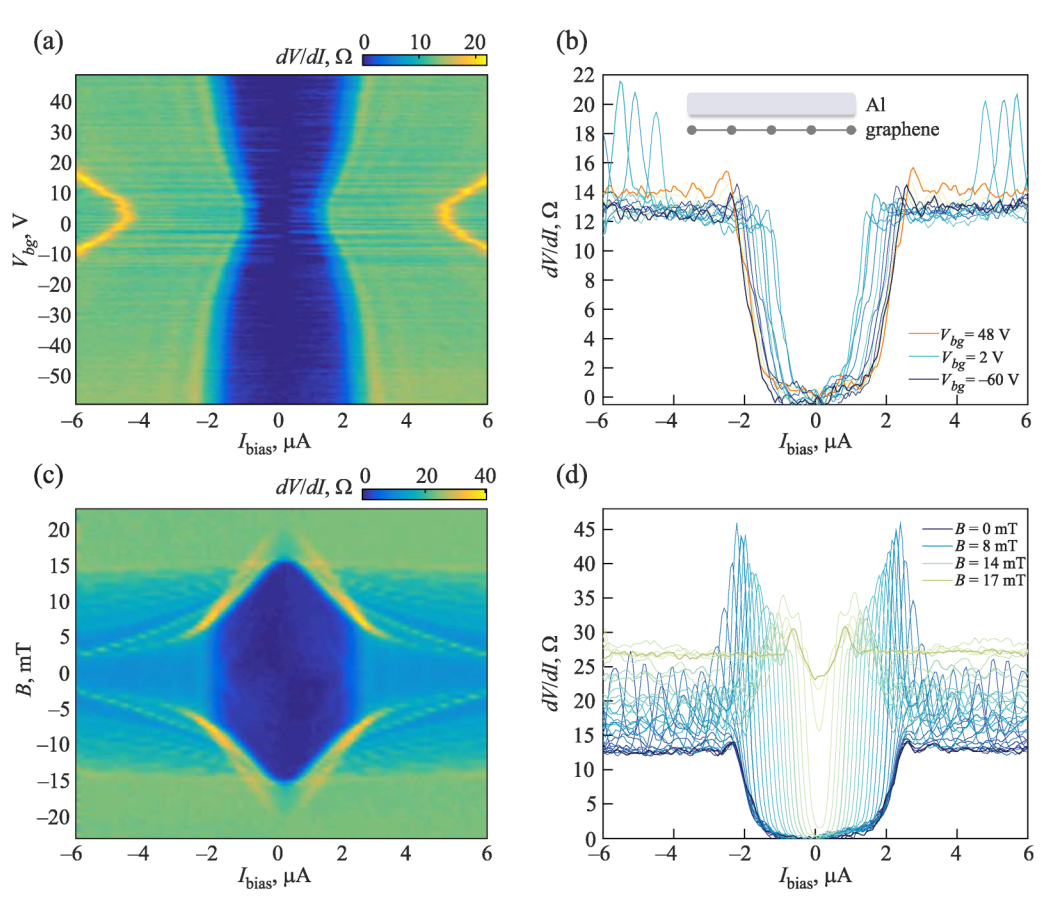


FIG. 2. (a) Gate dependence of tunneling resistance dV/dl in the strongly coupled regime. In the device, the graphene layer is in direct contact with Al. The color plot is dV/dl as a function of current bias (l_{bias}) and back-gate voltage V_{bg} . The gap in the bias current (the zero resistance region) can be tuned by a back-gate voltage and its minimum appears at the graphene Dirac peak ($V_{bg} = 3 \text{ V}$). (b) dV/dl as a function of at different V_{bg} , corresponding to the dotted horizontal lines in (a). (c) Magnetic field depend ence of the differential resistance dV/dl in the strongly coupled regime. The gate voltage is fixed at $V_{bg} = 50 \text{ V}$. (d) Several line cuts at constant magnetic fields B taken from (c). Inset figure shows the schematic diagram of the junction.

oscillations may occur if the Andreev reflected quasi-particles in the N region form coherent bound states due to the N region confinement (McMillan-Rowell resonance (MRR). 14-16 The mesoscopic size of both Al island and graphene channel in our device structures can in principle lead to these coherent oscillations on top of the superconducting states.

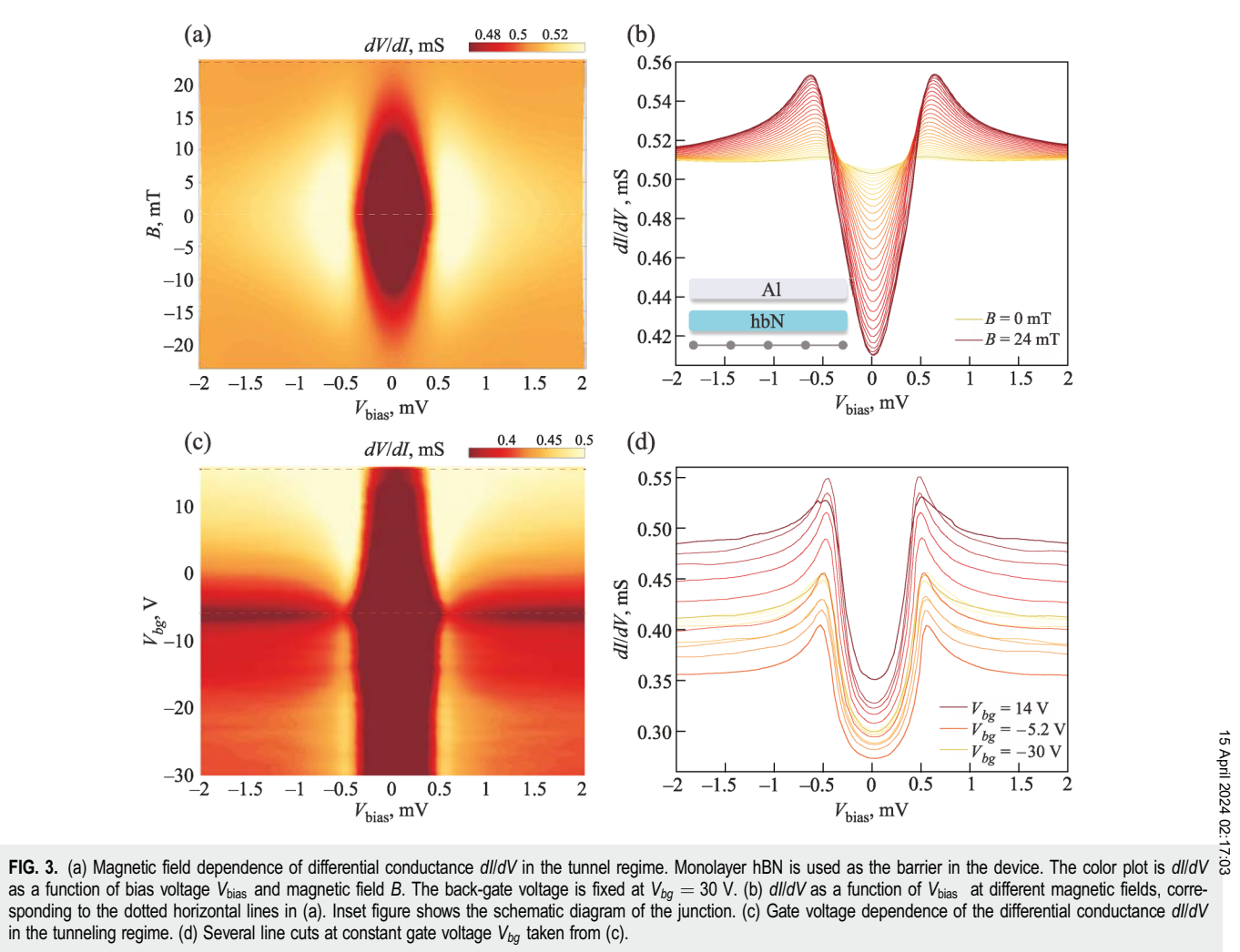
4. TUNNELING REGIME: AI/BN/GRAPHENE

In 2D materials research, hBN is commonly used as a dielectric substrate that provides a flat surface for graphene and can also screen the stray electric fields from the charged impurities within the silicon dioxide substrate. As a tunneling layer, hBN has been investigated extensively. There are numerous studies on the transmission probability between combinations of graphene/graphite/gold through different hBN layers. ^{17,18} In this section, we present the experimental results in such a system and explain them from

the perspective of Andreev process. Particularly, we focus on using one atom thick hBN monolayer in our devices.

Figure 3(a) shows the spectroscopic properties of the tunnel junction as a function of V_{ns} and magnetic field B at a fixed backgate voltage $V_{bg}=30$ V. We also plot the in-dividual line traces in Fig. 2(b) for 0 < B < 24 mT, extending above B_c . Tunneling conductance dI/dV shows a clear suppression for $|V_{ns}| < 0.7$ mV at low B, indicating the suppression of Andreev reflection due to the barrier, which decreases the transparency of the NS interface. The coherence peaks are seen at $V_{ns}:V_c=0.7$ mV, an energy which is considerably larger than the superconducting gap of Al ~ 0.25 mV. This may be due to a spurious voltage drop outside the junction area, which is picked up in our measurement configuration. Increasing B suppresses the superconductivity and at |B|=24 mT the tunneling conductance is constant in V_{ns} indicating the energy independent normal state conductance.

Figure 3(c) shows the tunneling conductance at B = 0 as a function of V_{ns} and V_{bg} The junction conductance is modulated by



in the tunneling regime. (d) Several line cuts at constant gate voltage V_{bq} taken from (c).

 V_{bg} , demonstrating that the graphene in the junction area is gatetunable. The conductance minimum at $V_{bg} \approx -7$ V observed for the entire measured energy range indicates the Dirac peak of the graphene. The line traces plotted in Fig. 3(d) show a suppressed tunneling conductance at small energies for the entire gate voltage range, which indicates that the back gate, while tuning the

TABLE I. Devices in the tunneling regime with different sizes of tunneling area. The R_N A product is consistent with the exponential dependence of zero-bias resistance on the thickness of hBN separating graphite and gold.

Device	Tunneling area, μm²	$R_{\rm N}$, $k\Omega$	$R_{\rm N}A$, $k\Omega\cdot\mu{\rm m}^2$
A	1.6	4.2	6.7
В	2.7	2.6	7.2
C	0.75	11.4	8.5
D	1.9	8.9	16.9

conductance of the graphene channel, does not significantly alter the junction transparency dictated by the barrier.

The hBN barrier employed in this experiment is monolayer, the thinnest barrier limit for this material. Nevertheless, we observe the conductance suppression, suggesting that the hBN barrier always provide weak coupling between Al superconductor and graphene channel. We tested four de vices with monolayer hBN as the barrier with different tunneling area A. We find that the tunneling resistance R_N in the normal regime (i.e., $|V_{ns}|\gg V_c$) is on the order of k Ω . The resistance area product (R_NA) in our devices is consistent with those in graphite/monolayer hBN/gold devices, 18 as shown in Table I.

5. INTERMEDIATE REGIME: AI/MoS₂/GRAPHENE

The weak coupling between Al and graphene channel across a large energy gap of hBN, as discussed in the previous section, can be turned into an intermediate coupling regime via replacing the vdW barrier in the device. In this section, we demonstrate the intermediate coupling regime by using a monolayer semiconducting TMD, MoS₂.

Figure 4(a) shows the resistance dV/dI in the intermediate transparency regime as a function of bias current I_{bias} and B at $V_{bg} = 60$ V. The characteristics are similar to that of the strongly coupled junction in Fig. 2(a) with the exception that, here, the junction resistance does not vanish at low bias current, suggesting that the graphene in the junction area is not completely proximitized [see line trac es in Fig. 4(b)].

Figure 4(c) shows the gate dependence of the tunneling differential conductance as a function of voltage bias at zero magnetic field. The Dirac point of the graphene channel is located around $V_{bg} = -55$ V, showing that the graphene channel is n-doped by being in contact with MoS₂. As shown in the traces in Fig. 4(d), when the Fermi level of graphene is away from the Dirac point, the dV/dI is strongly suppressed, indicating Andreev enhanced

conductance. As the gate voltage is tuned near the Dirac point, the junction turns into the weak coupling regime, losing most of the Andreev enhanced junction conductance at the zero bias limit.

Interestingly, the junction resistance at small $I_{\rm bias}$ changes in discrete steps as the magnetic field increases, evident from the line traces with several overlapping successively (labeled by the horizontal arrows). We will discuss these stepwise in crease of junction resistance in the next section.

6. MAGNETORESISTANCE PLATEAUS IN THE INTERMEDIATE REGIME

The discrete changes of Andreev current measured in Al/MoS₂/graphene device can be further investigated by sweeping magnetic fields at fixed bias voltage $I_{\rm bias}$ and gate voltage V_{bg} Fig. 5(a) shows the change of magneto resistance dR/dB as a function of $I_{\rm bias}$ and B at gate 60 V, taken from the same device in

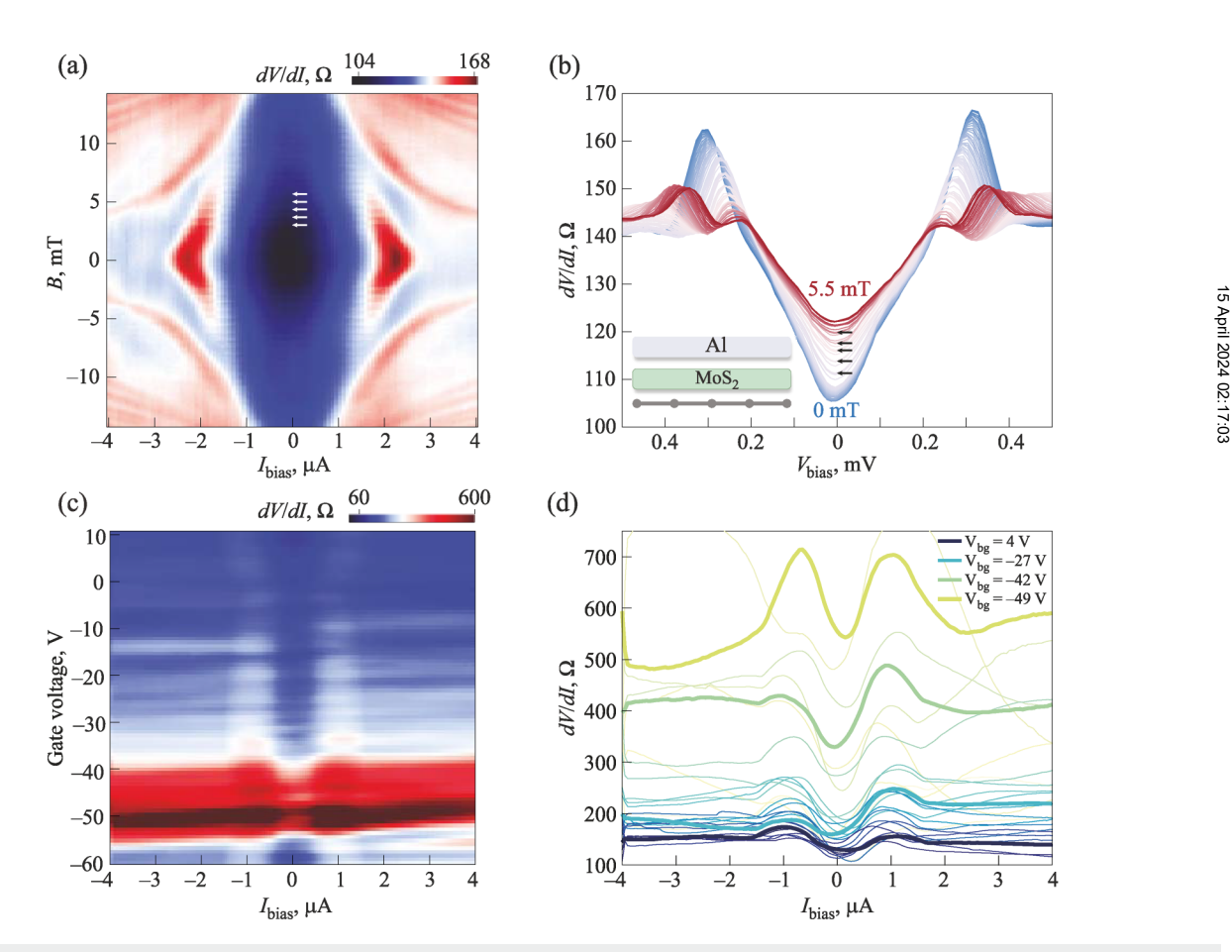


FIG. 4. (a) Magnetic field dependence of tunneling resistance dV/dl in the intermediate regime. The device has monolayer MoS₂ as the tunneling barrier. The color plot is dV/dl as a function of bias voltage ($V_{\rm bias}$) and magnetic field B. The backgate voltage is fixed at $V_{\rm bg} = 60$ V. The step features are indicated by the white arrows. (b) dV/dl as a function of $I_{\rm bias}$ at different magnetic fields, taken from (a). The magnetoresistance plateaus are manifested as these cuts from different B fall on top of each other within the low bias region, leaving only a few distinguishable lines (marked by the arrows). Inset figure shows the schematic diagram of the junction. (c) Gate voltage dependence of the differential resistance dV/dl. (d) Several line cuts at different gate voltages, taken from (c).

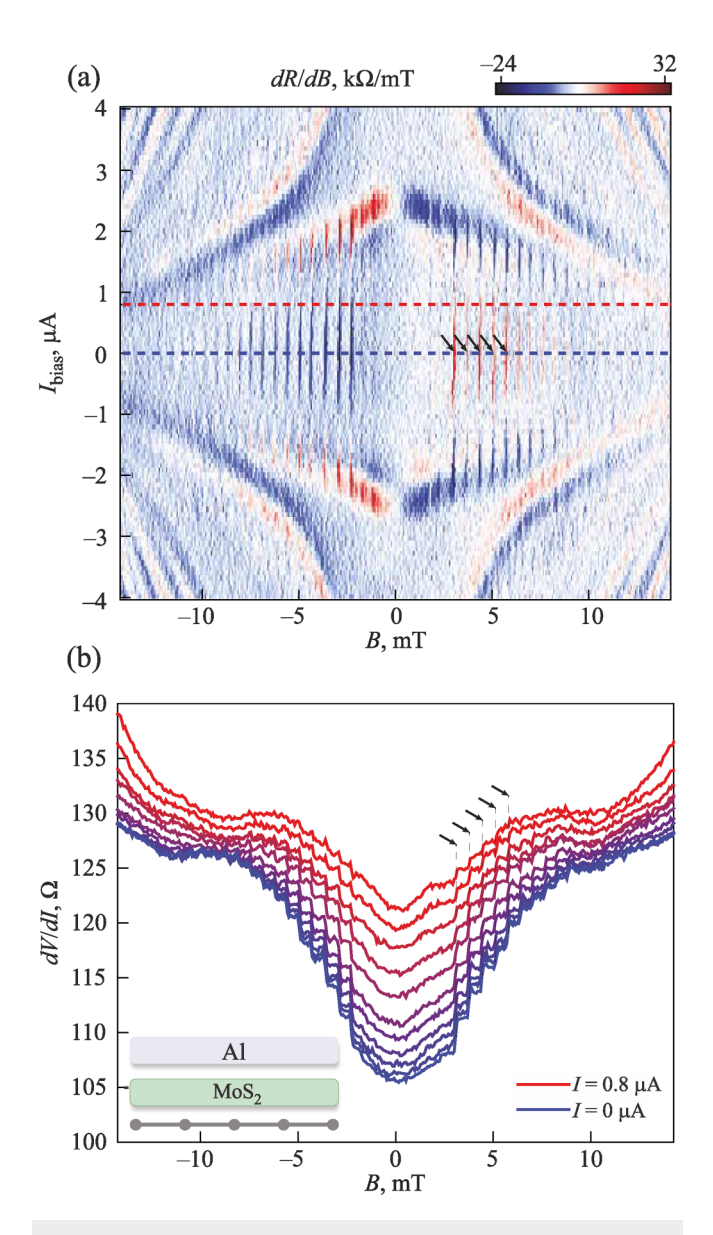


FIG. 5. (a) dR/dB as a function of magnetic field B and current bias $I_{\rm bias}$, where R is differential resistance R = dV/dI obtained in Fig. 4(a). Gate voltage is fixed at $V_{bg} = 60$ V. The black arrows mark the magnetic field values where sudden change of R occurs. (b) dV/dI as a function of B taken at various bias currents A (the range is marked by two horizontal lines in Fig. 5(a). The step features in dV/dI are evident at fixed magnetic field values, marked by the dashed lines and arrows.

similar transparency, (2) the slope of the steps changes sign (from measurement conditions presented in Fig. 4. Here, the differential resistance R = dV/dI is measured first using B as a fast sweeping variable while keeping $I = I_{\text{bias}}$ fixed during the measurement [see Fig. 5(b)]. This experimental procedure ensures that there is no experimental artifact such as flux jumping in the solenoid magnet

being used in the experiment. The steps in dV/dI are formed as B is varied and appear as the sharp peaks or dips in dR/dB, as shown in Fig. 5(a). This stepwise change of R is not seen at large I and B, suggesting these features have a super conducting origin. Figure 5(b) shows dV/dI as a function of B taken at various bias currents $I = 0 \dots 0.8 \mu A$. The step features appear at identical B values for all plotted I, indicating that these steps are reproducible and regularly spaced with a separation $\Delta B \approx 0.6 \mathrm{mT}$.

We have studied the observed resistance steps in sever-al devices as a function of magnetic field and gate voltage. Figure 6(a) shows the dI/dV traces at zero bias as a function of B for different devices with intermediate junction transparency. All the resistances change in steps, high lighted by arrows. While the visibility of the steps decreas es as the magnetic field increases, the periodicity of the steps remains constant for each device. This is shown in the Inset of Fig. 6(a), in which the positions of the steps in B are plotted against the index of the steps n, presenting a lin ear relation. The constant periodicity of the steps for each device suggests an origin of the steps, which is related to the junction area. The average magnetic field spacing ΔB then can be obtained from the slope of these linear lines.

We find that ΔB is directly related to the junction area of the device. Figure 6(b) shows the relation between $1/\Delta B$ and the area A of each device. Among the 4 devices measured in the intermediate coupling limit, shown in the lower Inset of Fig. 6(b), we find a linear relation between $1/\Delta B$ and the area A, implying that the steps originate from flux penetration through the junction. Indeed, the inverse slope of these linear line corresponds well with the superconducting magnetic flux quanta $\Phi_0 = h/2e$, as shown in the solid line in this graph.

While the step width in ΔB can be explained in terms of flux penetration into superconducting islands, the step height in dV/dE depends on the gate voltage. Figure 6(c) main panel shows dV/dE of device C measured as a function of V_{bg} at B=0. The colored squares indicate the value of V_{bg} for the four traces of dV/dI as a function of magnetic field, shown in Fig. 6(d). For each trace, we have marked with arrows the resistance values at which the steps appear and plotted them as a function 1/B, shown in the Inset of Fig. 6(c). The resistance values decrease is inversely proportional to B for each shown gate voltage.

We now discuss the physical origin of our observed resistance steps, which occur due to flux penetration through the junction. Our main observations are (1) the resistance steps are found only for the junctions with intermediate transparency, (2) the slope of the steps changes sign (from ascending to descending and vice versa) at finite bias, (3) the step height changes with gate voltage, and finally (4) the resistance value at which the steps appear decreases inversely proportional to *B*. These observations are consistent with vortex penetration into an Al contact that is thin enough to exhibit type II superconductor behaviors. In this explanation, each vortex penetrating the supercon ductor results in an abrupt change in the junction resistance.

Superconducting vortices have been directly observed in proximities of normal regions. ¹⁹ Due to the relation between the step width and graphene/Al overlapping area, we deduce the plateau feature is related to the transport of vortices at the interface as well as in the proximities of graphene. Although Al is a type I

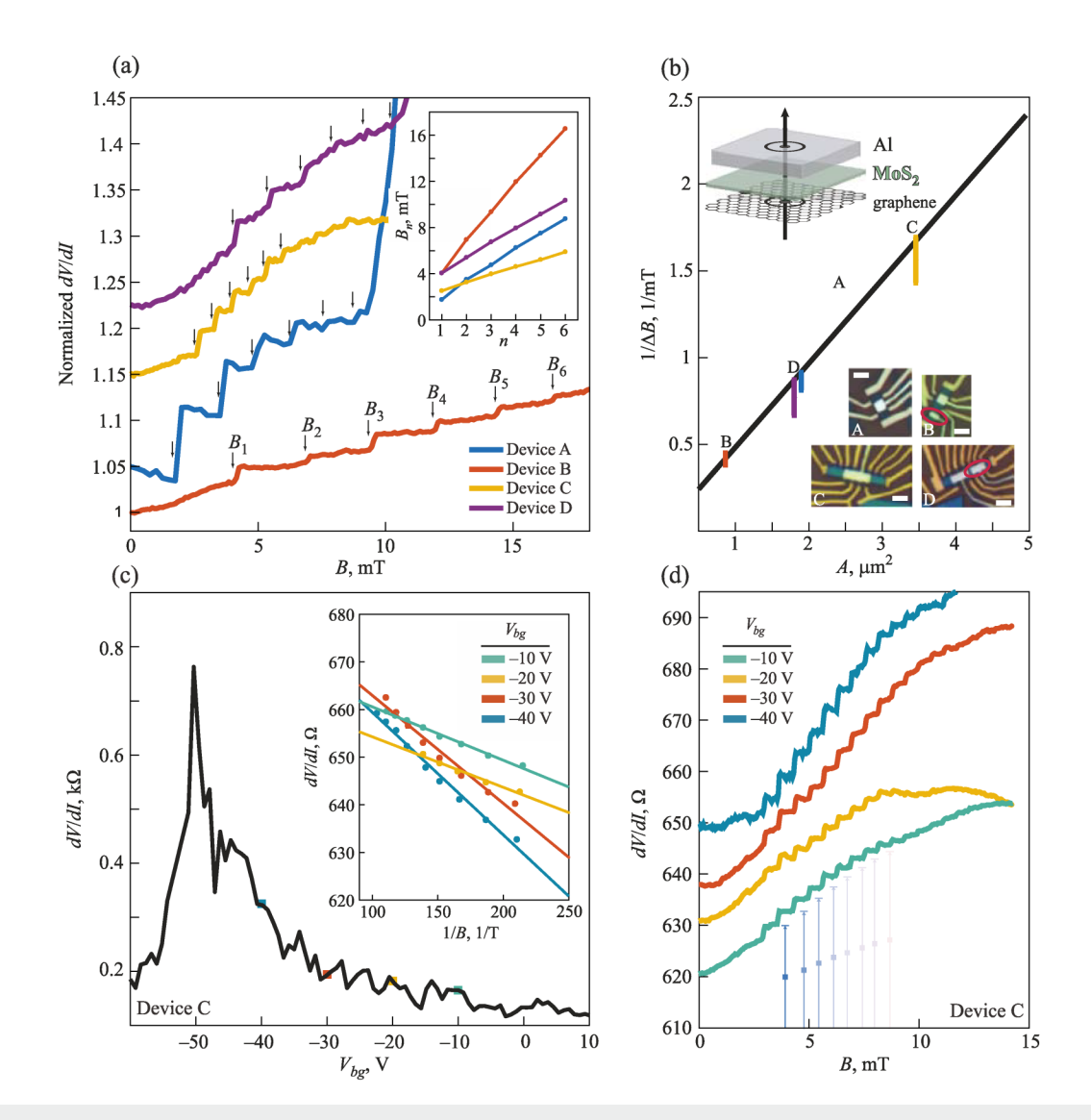


FIG. 6. (a) Step features in different devices. Inset shows Bn for each device; the slope provides the average step size, ΔB . (b) ΔB versus the device area A for four devices in the intermediate coupling regime. The lower Insets show optical microscope images of the devices. The solid line is for $\Delta BA = \Phi_0$. (c) Graphene channel resistance as a function of back-gate at zero magnetic field. Dirac peak of the graphene is at $V_{bg} = -50$ V. Dots with different colors correspond to the gate voltage where magnetic resistances are measured in (d). Inset displays the scattered data points with the value of each differential resistance step plotted as a function of 1/B, which shows a linear behavior. These slopes are gate-dependent. (d) dV/dI plateaus at different values of back-gate voltages. There is no clear step feature when graphene is at the charge neutrality point.

superconductor, which does not allow the formation of quantized magnetic vortices in the bulk sample, mesoscopic Al islands can exhibit vortex structures in the low magnetic field regime. ^{20,21}

Decreasing step height dV/dI with increasing magnetic field was reported in previous experiments that detected vortices in mesoscopic Al superconductors. In this work, current-driven splitting of multiquanta vortices are realized, where current-induced transitions between degenerate quantum states provide detectable junction resistance. Similarly, the gate voltage modulation of the step height in our devices could be related to the

gate voltage affecting the slope of the background resistance, which as a result determines the step height.

7. CONCLUSION

The Andreev process probability is determined by the barrier strength separating the normal conductor and the superconductor. In this paper, we explored the fundamental proximity effect in graphene systematically in different regimes depending on the Andreev probability. Using insulating van der Waals materials as

the tunnel barrier allows us to assemble a vertical structure with atomically flat and clean interface between graphene and the tunnel barrier. We can control the barrier strength by choosing materials with different sizes of band gap or different numbers of atomic layers. In the strongly coupled regime, i.e., without a barrier, we showed that when the superconducting Al is in direct contact with graphene, the induced gap is gate-tunable and there are above-gap features showing the superconducting correlation inside the graphene. However, the near zero resistance inside the gap prevents us from further probing the properties of proximitized graphene. Conversely, by using monolayer hBN as the barrier we enter the tunnel regime. The graphene is no longer proximitized and we can only observe the superconducting gap of Al without gate dependence and any above-gap features. An ideal regime for the purpose of our study is achieved by selecting monolayer MoS₂ as the separation layer between graphene and Al. In this intermediate regime, we find that inside the induced gap there is typically a 10-50% enhancement of conductance, indicating the predominance of the Andreev process between graphene and Al via MoS2. Furthermore, in the field dependence measurement there are plateaus developed in the magneto-resistance. Since the width of the plateaus is consistent with a flux quantum in the system, we ascribe their origin to

Our experimental results have demonstrated how to obtain different probabilities of the Andreev process by experimental control of vdW barrier strength. With significant probability of Andreev process, there is superconducting correlation in the graphene layer, and its proximity effect properties are characterized by the magnetic field as well as the carrier density.

Our experimental results have demonstrated how to obtain different probabilities of the Andreev process by experimental control of vdW barrier strength. With significant probability of Andreev process, there is superconducting correlation in the graphene layer, and its proximity effect properties are characterized by the magnetic field as well as the carrier density.

ACKNOWLEDGMENTS

We thank Gil-Ho Lee, Yuval Ronen for helpful discussions. K.-F.H. acknowledges support from NSF (DMR 2105048) for sample preparation and fabrication. Ö-.G. acknowledges support from a Rubicon grant from the Netherlands Organization for Scientific Research (NWO). P.K. acknowledge support from DOE (DE-SC0012260) for measurement and analysis, and NSF (QII-TAQS MPS 1936263) for characterization. K.W. and T.T. acknowledge support from the Elemental Strategy Initiative conducted by the MEXT, Japan (Grant No. JPMXP0112101001) and JSPS KAKENHI (Grant Nos. 19H05790 and No. JP20H00354). Nanofabrication was performed at the Center for Nanoscale Systems at Harvard, supported in part by a NSF NNIN Grant No. ECS-00335765.

REFERENCES

¹A. Andreev, J. Exp. Theor. Phys. 19, 1228 (1964).

²G. E. Blonder, M. Tinkham, and T. M. Klapwijk, Phys. Rev. B 25, 4515 (1982). ³V. E. Calado, S. Goswami, G. Nanda, M. Diez, A. R. Akhmerov, K. Watanabe, T. Taniguchi, T. M. Klapwijk, and L. M. K. Vandersypen, Nat. Nano 10(9), 761

⁴Y. Cao, V. Fatemi, S. Fang, K. Watanabe, T. Taniguchi, and E. Kaxiras, P. Jarillo-Herrero, Nature 556(7699), 43 (2018).

5G.-H. Lee, K.-F. Huang, D. K. Efetov, D. S. Wei, S. Hart, T. Taniguchi, K. Watanabe, A. Yacoby, and P. Kim, Nat. Phys. 13, 693 (7699), (2017).

⁶C. R. Dean, A. F. Young, I. Meric, C. Lee, L. Wang, S. Sorgenfrei, K. Watanabe, T. Taniguchi, P. Kim, K. L. Shepard, and J. Hone, Nat. Nano 5(10), 722 (2010).

⁷L. Wang, I. Meric, P. Y. Huang, Q. Gao, Y. Gao, H. Tran, T. Taniguchi, K. Watanabe, L. M. Campos, D. A. Muller, J. Guo, P. Kim, J. Hone, K. L. Shepard, and C. R. Dean, Science 342, 614 (2013).

⁸C. Lattyak, K. Gehrke, and M. Vehse, J. Phys. Chem. C **126**, 13929 (2022).

⁹K. Watanabe, T. Taniguchi, and H. Kanda, Nat. Mater. 3, 404 (2004).

¹⁰Y. Kubota, K. Watanabe, O. Tsuda, and T. Taniguchi, Science 317, 932 (2007). ¹¹A. K. Cheng, "Electric transport in hybrid carbon nanotube graphene devices", Ph.D. thesis, Harvard University (2019).

¹²W. J. Tomasch, Phys. Rev. Lett. **16**, 16 (1966).

13 W. L. McMillan and P. W. Anderson, Phys. Rev. Lett. 16, 85 (1966).

14C. Visani, Z. Sefrioui, J. Tornos, C. Leon, J. Briatico, M. Bibes, A. Barthélémy, J. Santamaría, and J. E. Villegas, Nat. Phys. 8, 539 (2012).

15J. M. Rowell and W. L. McMillan, Phys. Rev. Lett. 16, 453 (1966).

¹⁶J. M. Rowell, Phys. Rev. Lett. **30**, 167 (1973).

17 J. M. Rowell, Phys. Rev. Lett. 30, 167 (1973).

Rev. Lett. 30, 167 (1973).

Rev. Lett. 30, 167 (1973).

Rev. Lett. 30, 167 (1973). T. Taniguchi, and D. Goldhaber-Gordon, Phys. Rev. B 85, 073405 (2012).

¹⁸L. Britnell, R. V. Gorbachev, R. Jalil, B. D. Belle, F. Schedin, M. I. Katsnelson, L. Eaves, S. V. Morozov, A. S. Mayorov, N. M. R. Peres, et al., Nano Lett. 12, 1707 (2012).

19D. Roditchev, C. Brun, L. Serrier-Garcia, J. C. Cuevas, V. H. L. Bessa, M. V. Milošević, F. Debontridder, V. Stolyarov, and T. Cren, Nat. Phys. 11, 332

²⁰A. K. Geim, S. V. Dubonos, J. J. Palacios, I. V. Grigorieva, M. Henini, and J. J. Schermer, Phys. Rev. Lett. 85, 1528 (2000).

A. Kanda, B. J. Baelus, F. M. Peeters, K. Kadowaki, and Y. Ootuka, Phys. Rev. Lett. 93, 257002 (2004),

²²M. V. Milošević, A. Kanda, S. Hatsumi, F. M. Peeters, and Y. Ootuka, Phys. Rev. Lett. 103, 217003 (2009).